energies

MDPI

Article

LLC Resonant Converter as a Current Source Using Simple Trajectory Control

Tsvetana Grigorova [1,*] and Aleksandar Vuchev [2]

[1] Department of Electronics, Faculty of Electronics and Automation, Technical University of Sofia, Plovdiv Branch, 63 Sankt Petersburg Blvd., 4000 Plovdiv, Bulgaria
[2] Department of Electrical Engineering and Electronics, Technical Faculty, University of Food Technologies, 26 Maritza Blvd., 4002 Plovdiv, Bulgaria; avuchev@yahoo.com
* Correspondence: c_gr@tu-plovdiv.bg

Abstract: This paper discusses a simple method for controlling an LLC resonant DC-DC converter using a state space trajectory based on a linear combination of the voltage across the capacitor and the current through the inductance in the series resonant tank. An analysis of the converter using the state plane technique for the continuous current operation mode is proposed. The output, control and load characteristics of the converter, required for its design and application, are built for the different inductance ratios. They specify the limitations in the control range of the LLC resonant converter which result from the use of the control method. It is shown that under this control, the converter possesses linear control characteristics and has current source behavior. Therefore, the converter can successfully be used as a battery-charging device. Simulations of the converter's operation, both in steady state and when the control parameter is changed significantly, are implemented. Studies using the model confirm that the considered simple trajectory control provides a fast dynamic response and stable operation of the LLC resonant converter, even in cases of a significant change in the control.

Keywords: LLC resonant DC-DC converter; load characteristics; optimal trajectory control; state plane analysis

check for updates

Citation: Grigorova, T.; Vuchev, A. LLC Resonant Converter as a Current Source Using Simple Trajectory Control. *Energies* **2023**, *16*, 4629. https://doi.org/10.3390/en16124629

Academic Editor: Nicu Bizon

Received: 29 April 2023
Revised: 4 June 2023
Accepted: 7 June 2023
Published: 10 June 2023

Copyright: © 2023 by the authors. Licensee MDPI, Basel, Switzerland. This article is an open access article distributed under the terms and conditions of the Creative Commons Attribution (CC BY) license (https://creativecommons.org/licenses/by/4.0/).

1. Introduction

Resonant DC-DC converters operating above the resonant frequency are characterized by a high efficiency and an operational reliability. They are becoming an increasingly preferred source of high-frequency power for the needs of various industrial applications such as renewable energy applications [1], contactless energy transmission systems [2], electric vehicle applications [3,4], etc. LLC resonant converters, which are part of the resonant converters, have been widely discussed in recent years due to the advantages they possess and possibilities for applications in EV chargers [5,6], LED lighting applications [7–9] and various other applications [10]. An important design advantage of LLC topologies over other types of resonant converters is the possibility to implement the two inductances (series and parallel) practically in only one component, the matching transformer [11].

Many of the properties and characteristics of LLC resonant DC-DC converters are determined by the methods used for their control [12]. Widely used is the output power control method, based on changing the control frequency of the transistors in the inverter part of the circuit [13]. The frequency control method (FM) is easy to implement and can handle discontinuous currents, but it is characterized by slow dynamic response. Phase-shift control is another usable control method [14–17]. It is also easy to implement and allows operation at a constant frequency, but the efficiency is lowered at high loads. In [18], a disturbance-observer-based control for phase-shift LLC converters was introduced to improve the dynamic performances under large input voltages and load variations due to the strong nonlinearity of the LLC converter and difficulties using typical linear control methods.

Some authors propose using hybrid control methods to overcome the disadvantages of the FM and phase-shift control strategies. In [12,19], an LLC resonant DC-DC converter for a hybrid power system was considered, controlled by a frequency modulation and phase-shift control strategy. According to [20], a hybrid control method was also discussed that combines FM mode and PWM mode depending on the load conditions.

Another strategy, named the Bang-Bang Charge Control method for LLC resonant converters, was presented in [21]. The series capacitor voltage and a pair of threshold voltages were used to determine the switching instants of the transistors. The method provided sub-optimal trajectory since the controller did not calculate the new steady state. Fast feedback was used to bring the converter closer to the new steady state.

However, to achieve a fast transient response, an optimal trajectory control method was initially performed in [22] for series resonant converters. Due to the increased number of state variables and operating modes in the LLC converter circuit, this control is more complicated to implement. In [23], an application of the optimal trajectory control method for LED PWM dimming was presented.

Optimal trajectory control has several advantages compared with the other control methods: a reduction in overvoltages of reactive and switching elements in the circuit, and fast dynamic response in cases of significant changes in converter operating conditions without affecting the stability of the whole system. A disadvantage of the method is the necessity to calculate in real time a nonlinear function that defines all the energy stored in the resonant circuit.

In [24,25], a simplified optimal trajectory control for LLC converters was presented by assuming that the switching frequency equaled the resonant frequency. Thus, very fast dynamic performances were achieved, but the influence on the operation at other switching frequencies needs to be discussed.

A simple control method for a series resonant converter was proposed in [26] to achieve characteristics similar to an optimal trajectory controlled converter. At the same time, it reduced the complexity of this control technique. The significant simplification of the discussed control technique was mainly due to the linearization of the control function around the switching point.

On the basis of this concept, the present article proposes a simple trajectory control for an LLC resonant converter, ensuring a behavior similar to that with optimal trajectory control. Furthermore, the large number of state variables usually used for implementing optimal trajectory control in LLC resonant converters is reduced, and the control technique is simplified.

The main objective of the paper is the study converter's behavior by obtaining normalized output, control and load characteristics operating above its series resonant frequency. These characteristics, required for the LLC resonant converter design and application, are built for the different inductance ratios. The boundaries, at which the simple trajectory control method is valid, are defined. A functional model of an LLC resonant converter controlled by the considered method is presented and implemented using the principle of Analog Behavioral Modeling (ABM) embedded in the *PSpice for TI* simulator. A simulation of the converter's behavior is performed and compared with the analytically obtained results.

2. Converter Operation Using a Simple Control Technique

Figure 1 shows a circuit diagram of the considered full-bridge configuration of an LLC DC-DC converter. It consists of an inverter part (transistors $S_1 \div S_4$ and anti-parallel diodes $D_1 \div D_4$), a series resonant circuit (Ls and Cs), a parallel inductance L_P, a matching transformer (Tr), an uncontrolled rectifier ($D_5 \div D_8$), a capacitive output filter (C_0) and an output (V_0).

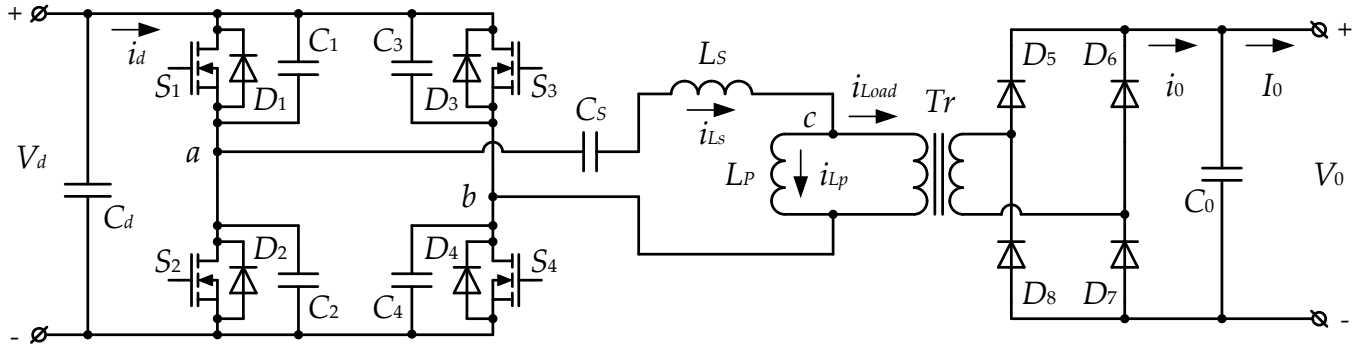


Figure 1. LLC resonant converter—a full-bridge configuration.

It was assumed that all elements in the circuit were ideal, the commutations in the inverter and rectifier were instantaneous and the ripple of the supply V_d and output V_0 voltages were negligible. The matching transformer was also ideal and had a unity turns ratio k.

The ratio of the two inductances is expressed by the coefficient a:

$$a = L_P/L_S. \tag{1}$$

If the inductance L_P in the parallel branch of the storage circuit has an infinitely large value ($a = \infty$), the circuit of the well-known series resonant converter (SRC) is obtained.

According to the assumptions made, the resonant frequency ω_0 and the characteristic impedance Z_0 of the series resonant circuit are determined as follows:

$$\omega_0 = 1/\sqrt{LsCs} \text{ and } Z_0 = \sqrt{Ls/Cs}. \tag{2}$$

The converter operates at a frequency ω_S that is higher than the natural frequency ω_0 of the series resonant circuit (L_S, C_S), thus defining a frequency ratio $\nu = \omega_S/\omega_0 > 1$.

For the purposes of the discussed control technique, as well as for obtaining generalized results, it is necessary to normalize all quantities characterizing the converter's performance as follows: voltages with the voltage factor V_d; currents with the current factor V_d/Z_0. The following quantities are denoted in relative units:

- Normalized output voltage V'_0

$$V'_0 = kV_0/V_d, \tag{3}$$

- Normalized output current I'_0

$$I'_0 = \frac{I_0/k}{V_d/Z_0}, \tag{4}$$

- Normalized input current I'_d

$$I'_d = \frac{I_d}{V_d/Z_0}, \tag{5}$$

- Normalized output power P'_0

$$P'_0 = I'_d = \frac{V_0 I_0}{V_d^2/Z_0}. \tag{6}$$

For resonant converters, the analysis was performed based on the behavior of the stored circuit. Therefore, the normalized values of the voltage v'_{Cs} across the capacitor Cs and the current i'_{Ls} through the inductance Ls are chosen as the state variables:

$$v'_{Cs} = v_{Cs}/V_d \quad and \quad i'_{Ls} = i_{Ls}/(V_d/Z_0). \tag{7}$$

At any time instant, these variables define a representative point. It is known that at steady state, this point will describe a closed "operating" trajectory composed of arcs of four circles.

2.1. Simple Control Method for a Series Resonant Converter

As mentioned previously, if the inductance L_P in the parallel branch of the energy storage circuit has an infinitely large value ($a = \infty$), the LLC converter behaves like of the series resonant converter (SRC).

The simplified control of SRC proposed in [26] was based on a circuit's behavior similar to that with optimal control of the operating trajectory. The significant simplification of the control was due to the use of a linear control law, describing a linear combination of the voltage across the capacitor and the current through the inductance in the series resonant circuit. The nature of the method is illustrated using Figure 2, where a trajectory described by the steady-state representative point is presented.

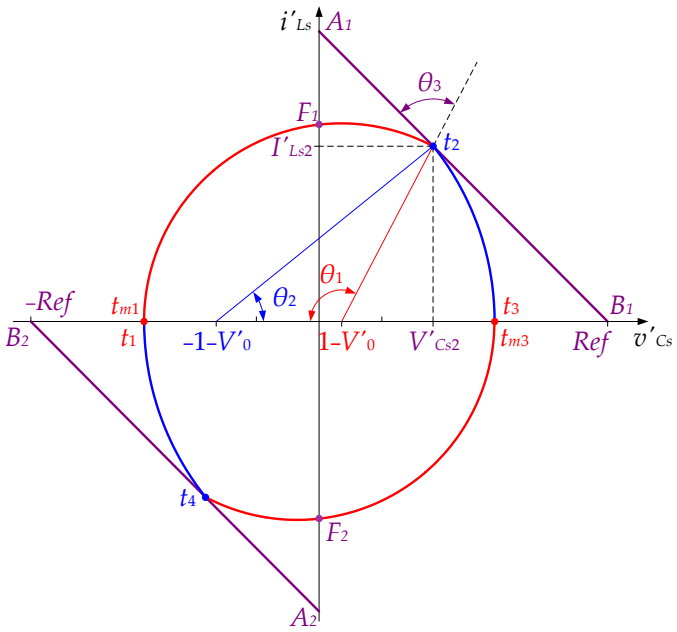


Figure 2. Steady-state phase plane representation at inductance ratio $a = \infty$.

The trajectory is composed of four arcs whose centers lie on the abscissa. The first arc has a center with coordinates $(1–V'_0, 0)$ and angle θ_1. It corresponds to the transistors' (S_1, S_3) conduction interval. It starts at point $t_1(V'_{Cs1}, I'_{Ls1})$ and ends at point $t_2(V'_{Cs2}, I'_{Ls2})$, respectively. Initially, the current through the series inductance is zero ($I'_{Ls1} = 0$), and the voltage across the capacitor acquires a negative peak value ($V'_{Cs1} = -V'_{CsM}$). The second arc has a center with coordinates $(-1–V'_0, 0)$ and an angle θ_2. It corresponds to the conduction interval of the freewheeling diodes (D_2, D_4). It starts at point $t_2(V'_{Cs2}, I'_{Ls2})$ and ends at point $t_3(V'_{Cs3}, I'_{Ls3})$, respectively. Now, $I'_{Ls3} = 0$ and $V'_{Cs3} = V'_{CsM}$. The other two arcs describe the operation in the next half-period. As expected, their centers are located mirror to the ordinate. For the third arc, which corresponds to the conduction of the switches (S_2, S_4), the center has coordinates $(-1 + V'_0, 0)$. The center of the fourth arc is given by coordinates $(1 + V'_0, 0)$. It corresponds to the conduction interval of the freewheeling diodes (D_1, D_3). Accordingly, the first and third arcs have the same radii and angles. Analogically, the second and the fourth arcs have equal radii and angles. Therefore, the coordinates of point $t_4(V'_{Cs4}, I'_{Ls4})$ will be symmetric to point $t_2(V'_{Cs4} = -V'_{Cs2}, I'_{Ls4} = -I'_{Ls2})$. Furthermore, the following equation is valid for the angles of the arcs:

$$\theta_1 + \theta_2 = \pi/\nu. \tag{8}$$

Obviously, the turn-on instants of the transistors are always on the abscissa because the current in the resonant circuit i_{Ls} changes its direction, and MOSFETs' body diodes are switched off. The switching of the rectifier diodes ($D_5 \div D_8$) takes place at the same points. The transition of the representative point from the second to the first quadrant or from the fourth to the third quadrant is detected by the change in the sign of the variable v'_{Cs}.

The main idea of the considered control technique is to define one control line A_1B_1 (Figure 2) in the first quadrant (and one in the third quadrant - A_2B_2, respectively) in the plane specified by (7) and to turn the transistors off when the trajectory of the representative point hits these lines (points t_2 and t_4). Thus, the energy stored in the resonant tank is limited.

The equations describing the control lines are given by [26]:

$$i'_{Ls} = M\left(v'_{Cs} \mp Ref\right), \tag{9}$$

where M is the slope of the switching lines and Ref is the normalized control amplitude for adjusting the converter's output power. The "$-$" sign in front of the Ref parameter refers to the A_1B_1 line and the "+" sign to the A_2B_2 line. It is easily found that the two control lines "enclose" from the abscissa v'_{Cs} an area from $-Ref$ to + Ref.

2.2. Simple Control Method for an LLC Resonant Converter

On the basis of the analysis presented in [27], it can be concluded that the steady-state trajectory for an LLC resonant DC-DC converter in the continuous current mode is identical to those of the classical series resonant converter. Therefore, it is possible to apply the control technique proposed in [26], too.

Figure 3 presents the steady-state phase plane trajectory for an LLC resonant DC-DC converter at continuous current mode (CCM).

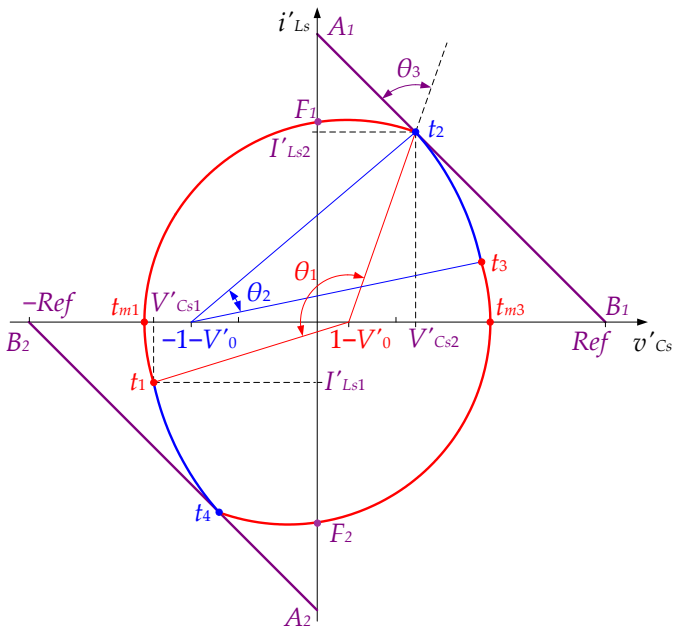


Figure 3. Steady-state phase plane representation for an LLC converter.

The trajectory is also composed of four arcs whose centers have the same coordinates as in the series resonant converter. However, point $t_1(V'_{Cs1}, I'_{Ls1})$ is now located in the third quadrant, and point $t_3(V'_{Cs3}, I'_{Ls3})$ is in the first. This is due to the influence of the parallel inductance L_P. The current i_{Load} (Figure 1) passes through zero at points t_1 and t_3 when the switching of the diodes in the rectifier ($D_5 \div D_8$) occurs. Nevertheless, the switching points of the transistors are always located on the abscissa, where the current in the resonant circuit i_{Ls} changes its direction, and the freewheeling diodes stop conducting.

For transistors (S_1, S_3), that takes place at point $t_{m1}(-V'_{CsM}, 0)$, and that for S_2–S_4 at point $t_{m3}(V'_{CsM}, 0)$, respectively. The transition of the representative point from the second to the first quadrant (point F_1) or from the fourth to the third quadrant (point F_2) is again detected by the sign change of the V'_{Cs} variable. Additionally, Equation (8) is valid for the angles of the arcs.

As in the case of SRC, the points, which represent the instants that correspond to the transistor's turn-off, remain in the first quadrant—point $t_2(V'_{Cs2}, I'_{Ls2})$—or the third quadrant—point $t_4(V'_{Cs4}, I'_{Ls4})$. Therefore, the control lines A_1B_1 in the first and A_2B_2 in the third quadrants (Figure 3) in the plane defined by (7) can also be determined from (9). Thus, it is proposed that switches turn off when the trajectory of the representative point hits these lines (points t_2 and t_4) too.

2.3. Implementation of the Control Method

A functional block diagram, illustrating the implementation of the considered simple control method for an LLC DC-DC converter, is presented in Figure 4. As mentioned previously, the control method is based on a linear combination of the voltage across the capacitor and the current through the inductance in the series resonant circuit.

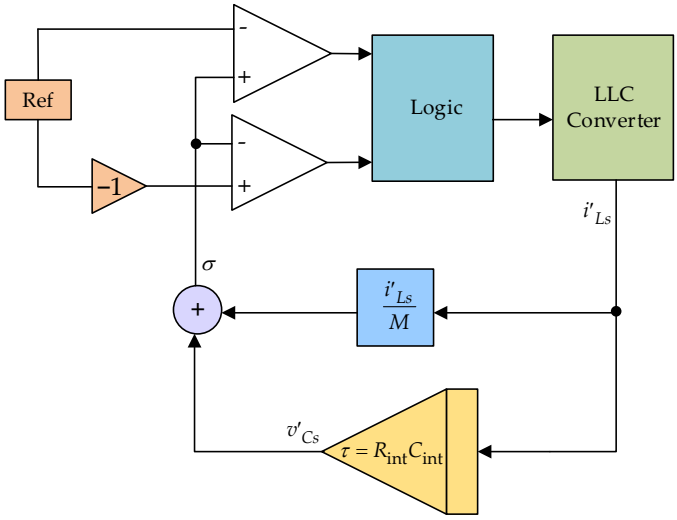


Figure 4. The functional block diagram of a simple control method for an LLC resonant converter.

A control variable σ, expressed in terms of the state variables v'_{Cs} and i'_{Ls}, is used to determine the switching instant of the transistors:

$$\sigma = v'_{Cs} - i'_{Ls}/M. \tag{10}$$

The switching off in the first quadrant (point t_2) occurs at $\sigma = +Ref$, and that in the third quadrant (point t_4) at $\sigma = -Ref$. It is accomplished using the two comparators and the logic circuit (Figure 4). Changing the value of the control parameter *Ref* will change the energy stored in the resonant circuit. With respect to determining the normalized values of the state variables in [26], it is proposed that the variable v'_{Cs} be determined from the current signal i'_{Ls} through the inductance *Ls*, via a passive integrating circuit. Moreover, no precise recommendations for the design of the integrating circuit are given. Hence, the solution to this problem is obtained as follows:

$$v'_{Cs} = \frac{V_{Cs}}{V_d} = \frac{\frac{1}{Cs}\int i_{Ls}dt}{V_d}\frac{Z_0}{Z_0} = \frac{1}{CsZ_0}\int i'_{Ls}dt. \tag{11}$$

The above equation shows that v'_C can be obtained based on variable i'_{Ls} simply via the integration circuit (Figure 4), whose time constant τ is defined as follows:

$$\tau = CsZ_0 = Cs\sqrt{Ls/Cs} = \sqrt{LsCs} = 1/\omega_0, \tag{12}$$

i.e., the time constant is reciprocal to the natural frequency of the series tank. Thus, the value of σ is uniquely determined based solely on the measurement of the current in the series resonant circuit.

In [26], the value of the angular factor was recommended to be $M = -1.0$. Thus, the normalized values of the voltage across the capacitor *Cs* and the current through the inductance *Ls* and their corresponding energies have an equal influence on the control.

Furthermore, the converter has the best dynamic behavior at this value of *M*. In the steady state, the trajectory of the representative point reaches the control lines every half-period. At these times, the corresponding transistor pairs are turned off. By changing the value of the parameter *Ref*, the resonant circuit's energy level and the trajectory type are changed, and the output power of the converter is regulated. The transition of the representative point from the second to the first quadrant (point F_1) or from the fourth to the third quadrant (point F_2) is detected by changing the sign of the variable v'_{Cs}. If the trajectory does not reach a control line, the switch pair continues to conduct until the current i'_{Ls} becomes equal to zero (points t_{m1} or t_{m3}). The next pair of switches starts conducting without freewheeling diodes previously conducted. Thus, the arc radii are increased during each subsequent half-period, which should result in the steady state being reached. However, as can be noticed, the proposed control can theoretically remain stable only when the following condition is satisfied:

$$\theta_3 \leq \pi/2. \tag{13}$$

Otherwise, the steady-state trajectory cannot reach the control lines. Hence, the converter will operate at a resonance concerning the series circuit (L_S, C_S). The occurrence of this "unstable" mode is determined on one side by the magnitude of the control parameter *Ref* and on the other side by the value of the output current I_0.

3. The Characteristics of the LLC Converter

In this paragraph, the output, control and load characteristics for an LLC converter controlled by the discussed algorithm are considered. Furthermore, the influence of the inductance ratio *a* on the circuit's characteristics is discussed. An analysis of a LLC DC-DC converter using the state plane technique was presented in [27]. The expressions for the fundamental quantities determined at steady-state operation of the LLC DC-DC converter with frequencies above the resonant frequency ω_0 of the series circuit (L_S, C_S) are given by:

- Normalized output voltage:

$$V'_0 = \frac{\sin\left(\frac{\pi}{\nu} - \theta_2\right) - \sin\theta_2}{\frac{\pi}{2a\nu}\left(1 + \cos\frac{\pi}{\nu}\right) + \sin\frac{\pi}{\nu}}. \tag{14}$$

- Normalized values of the currents and voltages at point $t_1(V'_{Cs1}, I'_{Ls1})$ and point $t_3(V'_{Cs3}, I'_{Ls3})$

$$I'_{Ls1} = -I'_{Ls3} = -\frac{V'_0\pi}{2a\nu}, \tag{15}$$

$$V'_{Cs1} = -V'_{Cs3} = \frac{-\frac{V'_0\pi}{2a\nu}\left(1 + \cos\frac{\pi}{\nu}\right) - 2\sin\theta_2}{\sin\frac{\pi}{\nu}} + 1 - V'_0 \tag{16}$$

- Normalized values of the currents and voltages at point $t_2(V'_{Cs2}, I'_{Ls2})$ and point $t_4(V'_{Cs4}, I'_{Ls4})$

$$V'_{Cs2} = -V'_{Cs4} = V'_0 V'_{Cs3}, \tag{17}$$

$$I'_{Ls2} = -I'_{Ls4} = \sqrt{(1 - V'_0 + V'_{Cs3})^2 + \left(\frac{V'_0\pi}{2a\nu}\right)^2} - (V'_0 V'_{Cs3} - 1 + V'_0)^2. \quad (18)$$

- Normalized maximum value V'_{CsM} of the voltage across the series capacitor Cs

$$V'_{CsM} = \sqrt{(1 - V'_0 + V'_{Cs3})^2 + \left(\frac{V'_0\pi}{2a\nu}\right)^2} - 1 + V'_0, \quad (19)$$

- Normalized average value of the output current I'_0

$$I'_0 = \frac{2\nu}{\pi} V'_{Cs3}. \quad (20)$$

- Normalized average value of the transistor current I'_{Sav}

$$I'_{Sav} = \frac{\nu}{2\pi}\left(V'_{CsM} + V'_0 V'_{Cs3}\right). \quad (21)$$

- Normalized average value of the freewheeling diode current I'_{Dav}

$$I'_{Dav} = \frac{\nu}{2\pi}\left(V'_{CsM} - V'_0 V'_{Cs3}\right). \quad (22)$$

The border between the continuous current (CCM) and discontinuous current (DCM) operating modes can be defined by the expression [28]:

$$-V'_{Cs1} + 1 - V'_0 = \frac{V'_0}{a}. \quad (23)$$

The above condition is fulfilled at $0 < \theta_2 \leq 0.5\pi/\nu$.

Using expressions (8), (9) and (13) ÷ (23), the relationships between the main quantities can be obtained to illustrate the properties of the resonant LLC DC-DC converter controlled by the investigated method under consideration in the continuous current mode. The main characteristics at inductance ratios $a = 1$, $a = 3$ and $a = \infty$ are plotted using the figures below. In the area of these dependencies, a stability border is visualized, where theoretically, for the minimum value of the output current, the trajectory of the operating point still reaches lines A_1B_1 and A_2B_2. It is determined by the condition defined by (13). Furthermore, for the cases $a = 1$ and $a = 3$, the CCM-DCM borderline (bright green) and the borderline based on the condition $\nu = \omega_S/\omega_0 = 1$ (gray) are shown.

Figure 5 shows the output characteristics $V'_0(I'_0)$ for values of the control parameter $Ref = 0.5 \div 5.0$ and the control characteristics $I'_0(Ref)$ of the converter for values of the normalized output voltage $V'_0 = 0.1 \div 0.9$.

On the basis of the waveforms given in Figure 5, it can be concluded that with the increase in inductance ratio a, the area of the discontinuous current mode decreases. Nevertheless, the stability border defines a theoretical possibility that when the control parameter Ref is varied over a wide range, the normalized output voltage reaches a relatively high value (≈0.8), which increases insignificantly when the inductance ratio a decreases.

Furthermore, the output characteristics are nearly concentric curves, with the distance between them being apparently proportional to the change in the control parameter Ref. When a short-circuit occurs, the converter remains operational, and also the value of the output current does not depend on the inductance ratio, since the parallel inductance has no influence.

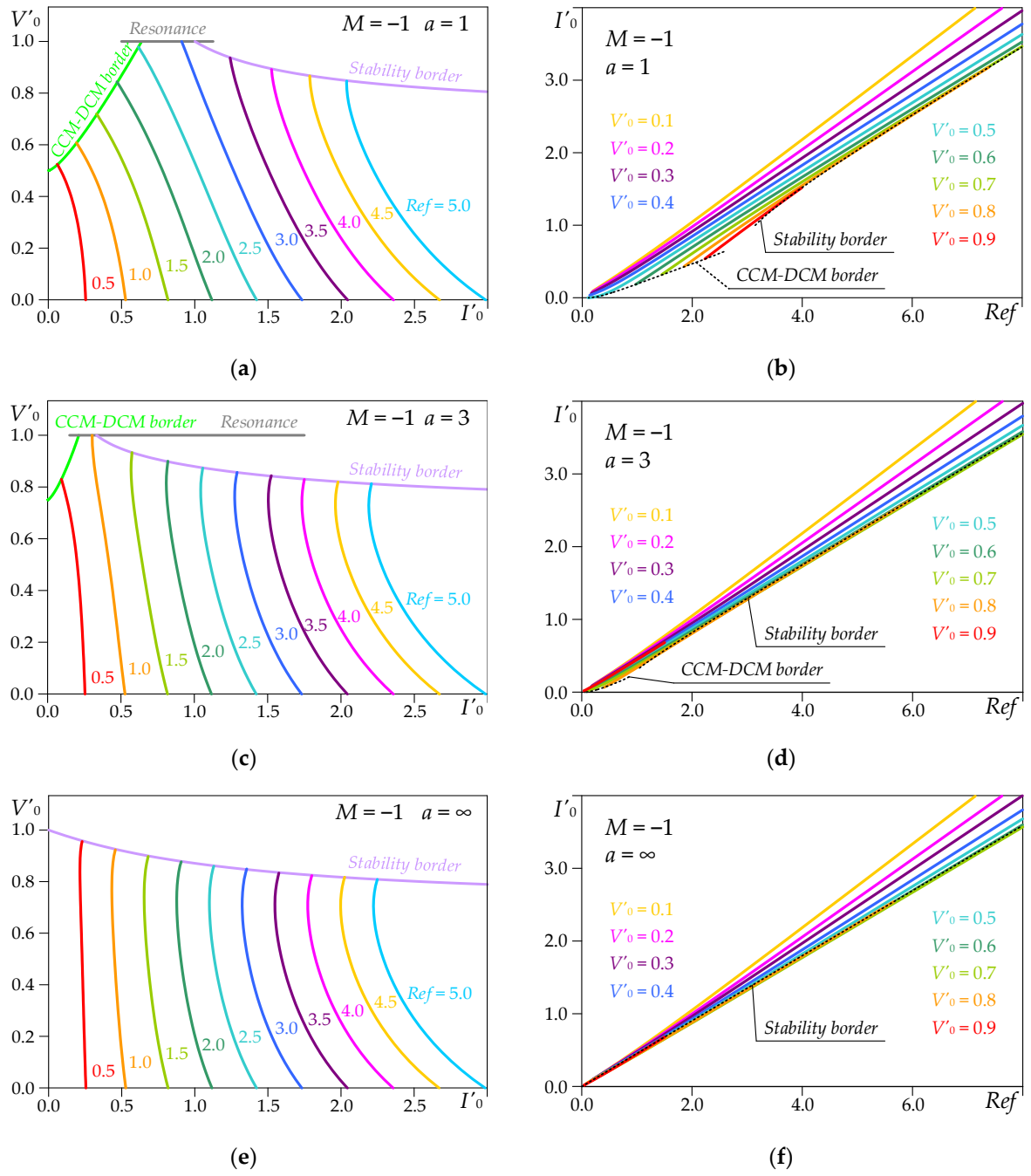


Figure 5. Output and control characteristics: (**a**) Output characteristics $V'_0(I'_0)$ for an induction ratio $a = 1$; (**b**) Control characteristics $I'_0(Ref)$ for an induction ratio $a = 1$; (**c**) Output characteristics $V'_0(I'_0)$ for an induction ratio $a = 3$; (**d**) Control characteristics $I'_0\ (Ref)$ for an induction ratio $a = 3$; (**e**) Output characteristics $V'_0(I'_0)$ for an induction ratio $a = \infty$; (**f**) Control characteristics $I'_0\ (Ref)$ for an induction ratio $a = \infty$.

It can also be noticed that for a relatively small value of the ratio $a = 3$, the output characteristics are obviously not significantly different from those of the series resonant converter ($a = \infty$).

The control characteristics $I'_0(Ref)$ are apparently linear for values of the control parameter $Ref \geq 1$. This can be easily explained by the concentric placement of output characteristics. From the results presented in Table 1, it can be reported that the dynamic coefficient $\Delta I'_0/\Delta Ref$ actually varies within a narrow range. It can be noticed that regard-

less of the magnitude of the inductance ratio, at low values of the normalized output voltage ($V'_0 = 0.1 \div 0.3$) the control characteristics practically coincide. In these cases, the largest variations of the dynamic coefficient are also taken into account. For high values of the normalized output voltage ($V'_0 = 0.6 \div 0.7$), the differences between the control characteristics at $a = 3$ and $a = \infty$ are insignificant. Those obtained at $a = 1$ deviate to a more significant degree.

Table 1. Values of the dynamic gain $\Delta I'_0/\Delta Ref$ at $Ref \geq 1$.

V'_0	$a = 1$	$a = 3$	$a = \infty$
0.1	0.52 ÷ 0.58	0.52 ÷ 0.58	0.52 ÷ 0.58
0.2	0.49 ÷ 0.54	0.49 ÷ 0.54	0.50 ÷ 0.54
0.3	0.47 ÷ 0.51	0.47 ÷ 0.51	0.48 ÷ 0.50
0.4	0.45 ÷ 0.49	0.45 ÷ 0.48	0.46 ÷ 0.48
0.5	0.45 ÷ 0.49	0.44 ÷ 0.47	0.45 ÷ 0.46
0.6	0.46 ÷ 0.50	0.44 ÷ 0.46	0.44 ÷ 0.45
0.7	0.46 ÷ 0.54	0.43 ÷ 0.45	0.43 ÷ 0.45

Figure 6 presents the basic normalized load characteristics of the converter required for its design at inductance ratios $a = 1$, $a = 3$ and $a = \infty$ for parameter values $Ref = 0.5 \div 5.0$. The dependences of the normalized average current through transistors I'_{Sav} and the normalized average current through diodes I'_{Dav} versus the output current I'_0 are plotted.

When a short-circuit across the converter's output terminals occurs, the values of I'_{Sav} and I'_{Dav} depend only on the magnitude of the parameter *Ref*. However, based on the reading taken of the stability border for the same magnitude of output current I'_0, they increase when decreasing the inductance ratio. This fact confirms a shortcoming of LLC converters. Namely, for the same magnitude of output current with a decreasing inductance ratio, the losses in the power devices of the inverter increase, resulting in a decrease in efficiency.

Figure 7 presents two other important normalized load characteristics obtained for inductance ratios $a = 1$, $a = 3$ and $a = \infty$ for parameter values $Ref = 0.5 \div 5.0$.

They are the dependences of the average value of the input current $I'_d(I'_0)$ and of the peak value of the voltage across the capacitor C_S of the series storage circuit $V'_{CsM}(I'_0)$ on the output current. The characteristics $I'_d(I'_0)$ demonstrate the variation in the converter output power ($P'_0 = I'_d$) by varying the parameter *Ref*, taking into account the influence of the inductance ratio *a*. It is clear that in case of a short-circuit of the converter output terminals, according to the assumptions adopted for the analysis, $P'_0 = 0$.

However, based on the reading taken of the stability border, it was observed that when *Ref* was changed from 3.5 to 5.0 the output power in relative units increased by approximately 1.49 times for $a = 1$. Respectively, for $a = 3$ this increase was 1.41 times and for $a = \infty$ it was 1.39 times. Therefore, even for low values of the inductance ratio, the considered circuit has very similar properties to those of a series resonant converter.

As for the other types of load characteristics, in case of a short-circuit across the output terminals, the peak value of the voltage across the capacitor C_S depends only on the parameter *Ref*. Based on the reading taken of the stability border at $Ref = 5$, $V'_{CsM} = 3.295$ for $a = 1$ and $V'_{CsM} = 3.266$ for $a = \infty$ can be reported. The difference is obviously not significant, and even for low values of the inductance ratio, the voltage stress on the capacitor was almost the same as that for a series resonant converter.

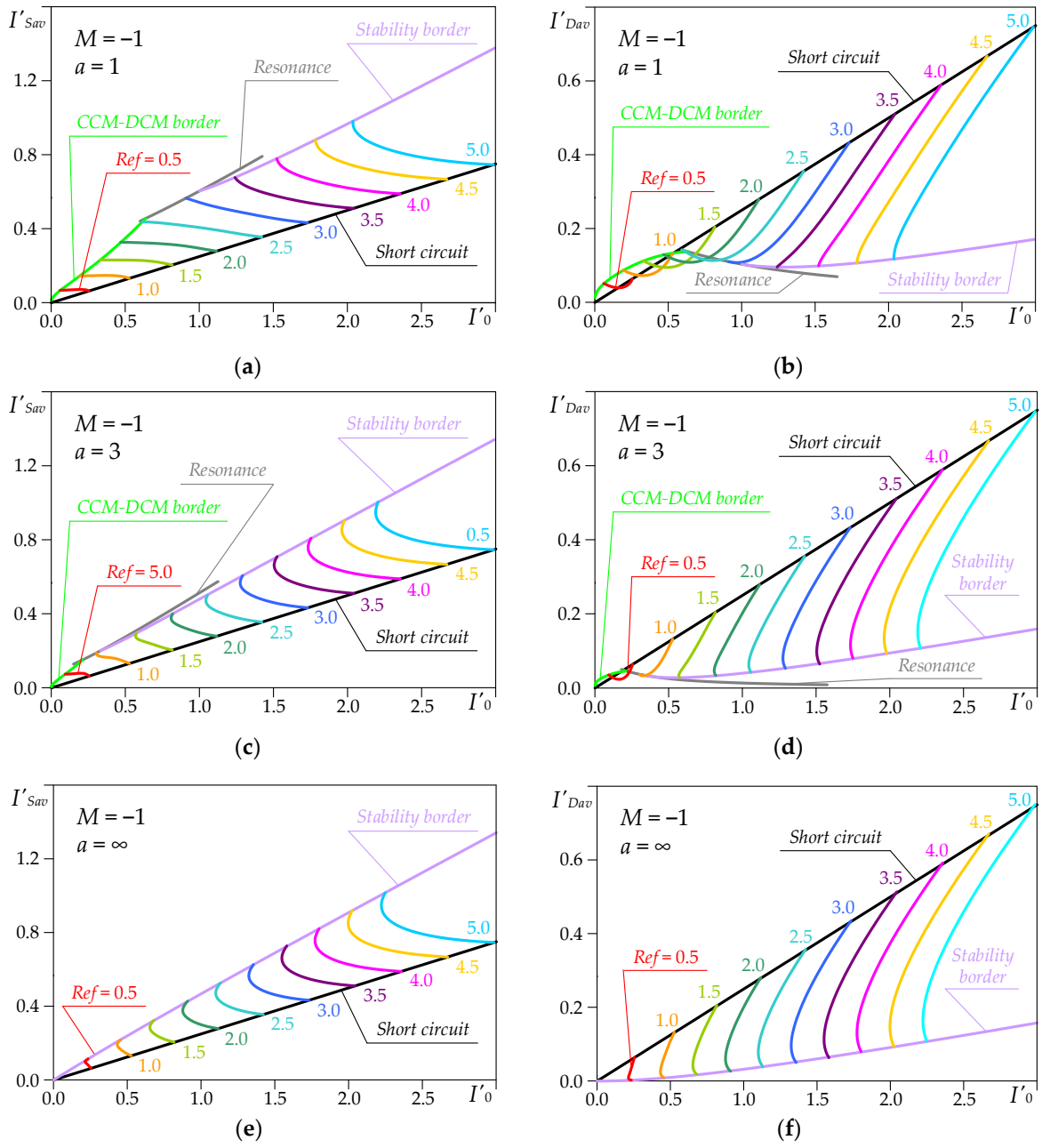


Figure 6. Load characteristics: (**a**) Normalized average transistor current I'_{Sav} vs. I'_0 for induction ratio $a = 1$; (**b**) Normalized average diode current I'_{Dav} vs. I'_0 for induction ratio $a = 1$; (**c**) Normalized average transistor current I'_{Sav} vs. I'_0 for induction ratio $a = 3$; (**d**) Normalized average diode current I'_{Dav} vs. I'_0 for induction ratio $a = 3$; (**e**) Normalized average transistor current I'_{Sav} vs. I'_0 for induction ratio $a = \infty$; (**f**) Normalized average diode current I'_{Dav} vs. I'_0 for induction ratio $a = \infty$.

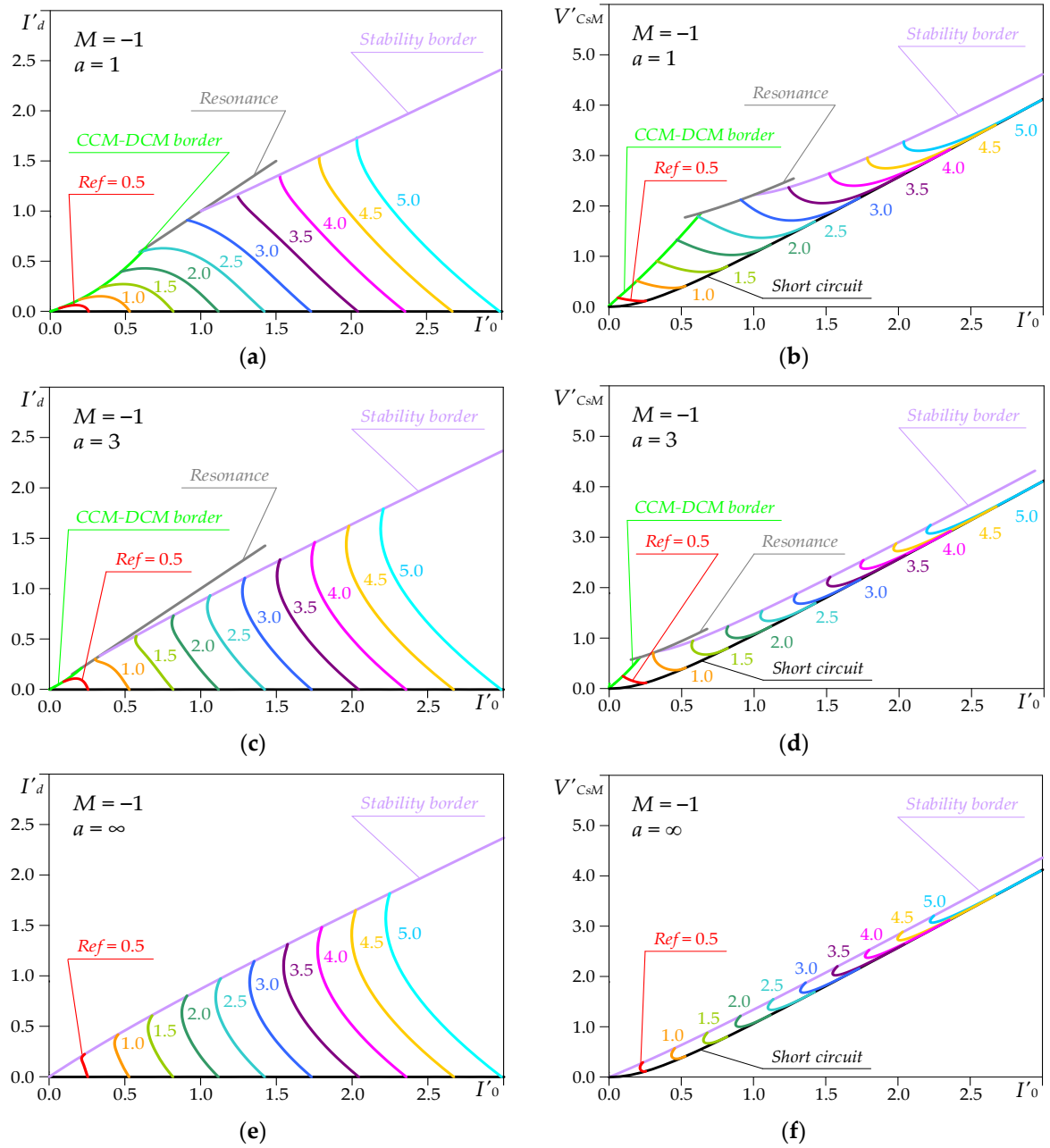


Figure 7. Normalized input current I'_d and normalized peak capacitor voltage V'_{CsM} vs. I'_0: (**a**) Normalized input current I'_d vs. I'_0 for induction ratio $a = 1$; (**b**) Normalized peak capacitor voltage V'_{CsM} vs. I'_0 for induction ratio $a = 1$; (**c**) Normalized input current I'_d vs. I'_0 for induction ratio $a = 3$; (**d**) Normalized peak capacitor voltage V'_{CsM} vs. I'_0 for induction ratio $a = 3$; (**e**) Normalized input current I'_d vs. I'_0 for induction ratio $a = \infty$; (**f**) Normalized peak capacitor voltage V'_{CsM} vs. I'_0 for induction ratio $a = \infty$.

4. Behavioral Modeling of the LLC DC-DC Converter Simple Trajectory Control Method

In order to verify the obtained analytical results, an LLC resonant DC-DC converter was designed with the following data: output power P = 1 kW; operating frequency f_S = 50 kHz; supply voltage V_{in} = 200 V; output voltage V_0 = 100 V. For the nominal operating mode, the frequency ratio was selected to be $\omega_S/\omega_0 = 1.15$. For the resonant circuit's elements, the following values were obtained: Cs = 88.56 nF; Ls = 151.306 µH; an

inductance ratio $a = 3$. The used MOSFET was IRF640, rectifier diodes were STTH1502D, the snubber capacitors' values were $C_{S1} \div C_{S4} = 1$ nF and the output capacitor was $C_0 = 10$ µF.

Figure 8 shows a simulation model of the investigated converter in the *PSpice for TI* environment [29,30]. The output includes a voltage source V_0 which simulates the connection of a battery. Each of the transistors M1 ÷ M4 was controlled by a ZVS driver with variable dead time [31] to be able to provide soft switching conditions over a wide load range. Through a current-controlled voltage source H1, signal ILL was obtained for the current through the resonant circuit.

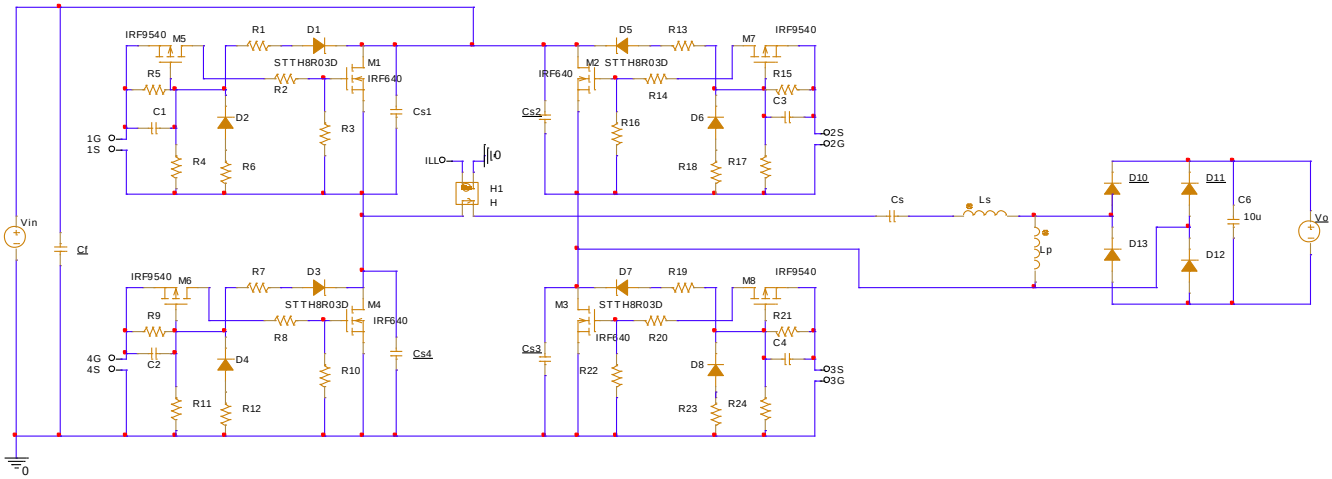


Figure 8. Simulation model of the LLC converter.

The converter's control system was described by the use of Analog Behavioral Modeling (ABM) embedded in a *PSpice for TI* simulator [29,30]. Thus, on the one hand, sufficiently accurate results were achieved and, on the other hand, the simulation process was simplified.

The driving pulses of transistors M1 ÷ M4 were controlled by a trigger circuit whose model is shown in Figure 9. In steady-state mode, the control pulses were fed to the driver circuits by the dependent voltage sources E1 ÷ E4. The duration of the shaped pulses was equal to one half-period. Following the considered control technique, the trigger circuit changed its state in the following cases:

- when the state trajectory (Figure 3) hit a control line (points t_2 or t_4), but not before the voltage sign changed (points F_1 or F_2);
- the state trajectory did not hit a control line when the current's sign changed (points t_{m1} or t_{m3}).

For these reasons, the following signals were applied to the trigger circuit: input B—turn-off in the first quadrant (along the trailing edge); input C—turn-off in the third quadrant (along the trailing edge); input D—voltage sign v'_C, input E—current sign i'_L. The signals at inputs D and E were inverted. They had low levels (logic zero) at positive values of the variables v'_{Cs} and i'_{Ls}. The proposed trigger circuit was simplified and contained fewer elements than the one presented in [26], yet fulfilled the same functions. The input signals for the trigger circuit were formed based on the current signal ILL and the control parameter *Ref* using a control circuit whose analog behavior model (ABM) is shown in Figure 10.

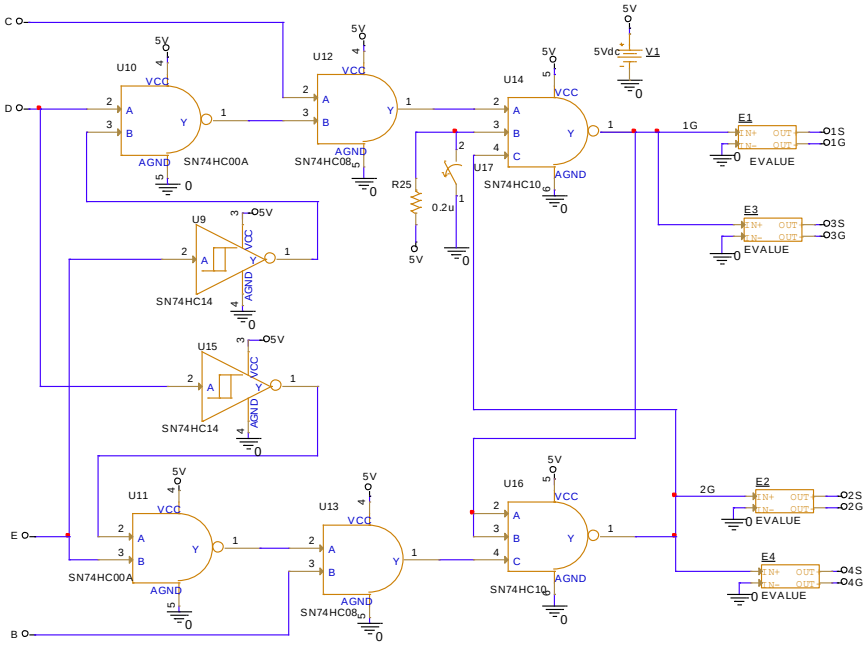


Figure 9. A model of the trigger circuit.

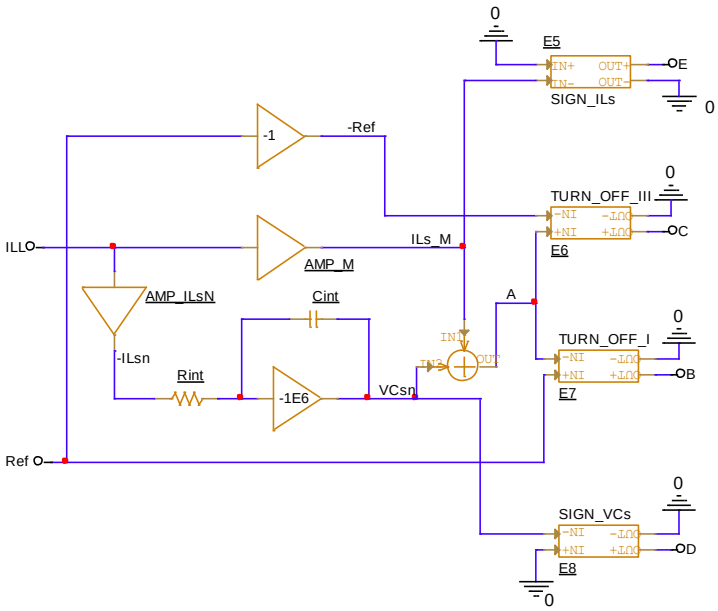


Figure 10. An ABM model of the control circuit.

An inverted signal for the variable i'_{Ls} was obtained via the AMP_ILsn amplifier. The second amplifier AMP_M formed the signal $-i'_{Ls}/M$ (ILs_M). Following Equation (11), an integrating amplifier formed a signal for v'_{Cs} (VCsn). A signal for the variable σ (A) was obtained by summing in the SUM block the signals VCsn and ILs_M according to (10).

Comparison blocks SIGN_ILs, TURN_OFF_III, TURN_OFF_I and SIGN_VCs forming the logic signals (E5 ÷ E8) applied to the inputs of the trigger circuit. Their gain coefficients were defined by expressions (7) and (10). The values of elements Rint and Cint were chosen to satisfy Equation (12). They were implemented by voltage-controlled voltage sources E5 ÷ E8, which describe the function:

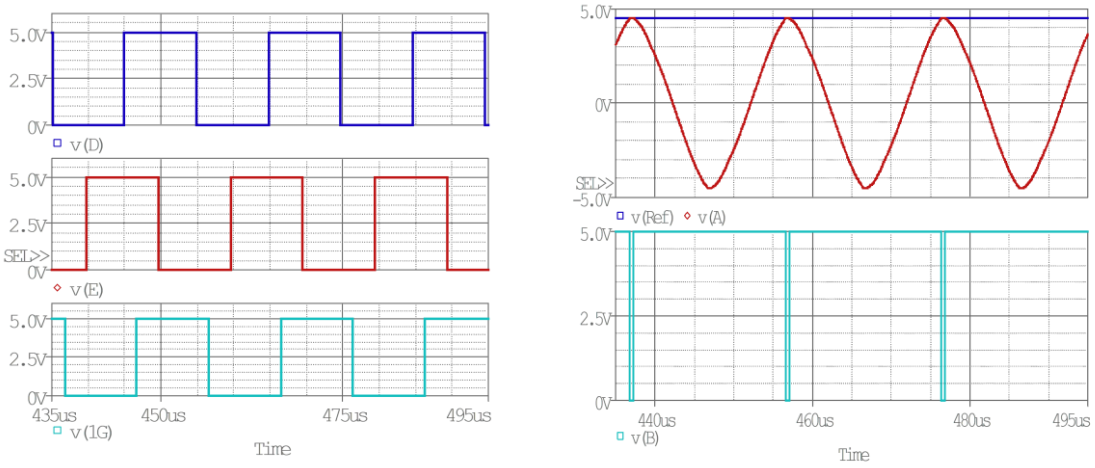
$$2.5*(\mathrm{SGN}(\mathrm{V}(\%\mathrm{IN}+, \%\mathrm{IN}-)) + 1). \quad (24)$$

An advantage of the proposed control circuit was in using easy-to-tune amplifier circuits to form the control variables.

5. Simulation Results

5.1. Steady-State Simulation Results

Simulation waveforms of the operation of the control circuit in steady-state mode are illustrated in Figure 11. Figure 11a shows the shaping of the control pulses for the given pair of transistors (S_1, S_3), which ended at positive values of the state variables (v(E) = 0 and v(D) = 0). At this point, the variable σ became greater than the control parameter *Ref* (V(A) > V(REF)) and the trailing edge of the signal applied to input B of the trigger circuit was formed (V(B) = 0)—as shown in Figure 11b. Thus, a change in the state of the trigger circuit occurred.



(**a**) (**b**)

Figure 11. Simulation waveforms of the control circuit signals (a = 3, *Ref* = 4.5): (**a**) From top to bottom—waveforms of the signals v(D), v(E) and v(1 G); (**b**) From top to bottom—waveforms of the signals v(REF), v(A) and v(B).

The output characteristics $V'_0(I'_0)$ obtained on the basis of expressions (8), (9), (13) ÷ (18) and (20) were verified for several values of the control parameter *Ref* = 1 ÷ 5 ($M = -1$ and a = 3). The theoretical results and those received from computer simulations were compared. The corresponding results are summarized in Table 2.

The deviations were usually within 2%. More significant differences (around 3%) were observed for small values of the control parameter *Ref*.

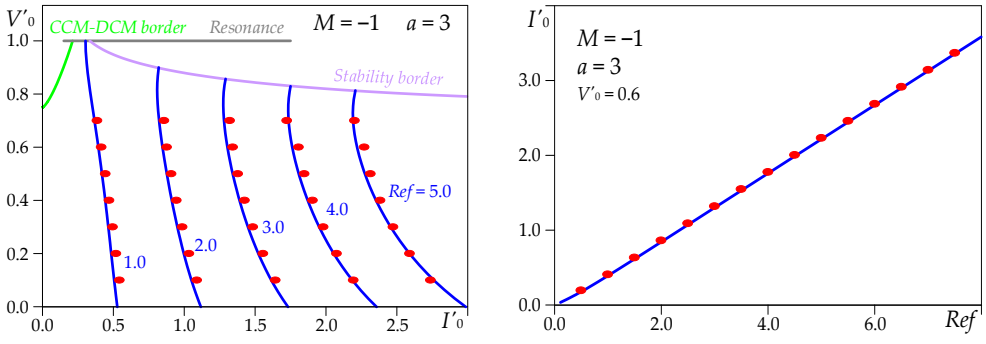
Similarly, a control characteristic $I'_0(Ref)$ obtained for V'_0 = 0.6 (the nominal normalized value of the output voltage) was verified for several values of the control parameter *Ref* = 0.5 ÷ 7.5 ($M = -1$ and a = 3). The corresponding results are summarized in Table 3.

The deviations between theoretical and simulation results did not exceed 2%. Larger differences were observed for small values of the control parameter *Ref*. A growing tendency of the relative error was observed as zero was approached.

Figure 12a shows a graphical representation of the results from Table 2 using dots (in red) in the area of output characteristics $V'_0(I'_0)$ and Figure 12b illustrates a graphical representation of the results from Table 3 using dots (in red) in the area of the control characteristics $I'_0(Ref)$.

Table 2. A comparison between theoretical and simulation results of output characteristics $V'_0(I'_0)$.

Control Parameter *Ref*	V'_0	I'_{0simul}	I'_{0calc}	Relative Error δ, %
Ref = 1	0.1	0.519	0.505	2.641
	0.2	0.495	0.485	2.257
	0.3	0.473	0.464	1.914
	0.4	0.449	0.443	1.453
	0.5	0.424	0.419	1.181
	0.6	0.397	0.394	0.784
	0.7	0.368	0.366	0.571
Ref = 2	0.1	1.072	1.050	2.031
	0.2	1.017	0.996	2.117
	0.3	0.971	0.951	2.054
	0.4	0.930	0.911	2.033
	0.5	0.894	0.876	1.994
	0.6	0.863	0.846	1.956
	0.7	0.844	0.822	2.693
Ref = 3	0.1	1.616	1.614	0.110
	0.2	1.530	1.523	0.477
	0.3	1.460	1.449	0.738
	0.4	1.402	1.389	0.919
	0.5	1.355	1.341	1.081
	0.6	1.320	1.304	1.250
	0.7	1.299	1.279	1.557
Ref = 4	0.1	2.190	2.185	0.208
	0.2	2.072	2.054	0.898
	0.3	1.978	1.951	1.356
	0.4	1.902	1.870	1.707
	0.5	1.844	1.807	2.056
	0.6	1.804	1.761	2.429
	0.7	1.721	1.735	−0.817
Ref = 5	0.1	2.733	2.760	−0.994
	0.2	2.586	2.587	−0.059
	0.3	2.469	2.456	0.557
	0.4	2.378	2.352	1.111
	0.5	2.310	2.273	1.602
	0.6	2.266	2.218	2.177
	0.7	2.198	2.190	0.369



(**a**) (**b**)

Figure 12. Verification of the theoretical results by means of computer simulations: (**a**) Verification of the output characteristics for $M = -1$ and $a = 3$; (**b**) Verification of the control characteristics for $M = -1$, $a = 3$ and $V'_0 = 0.6$.

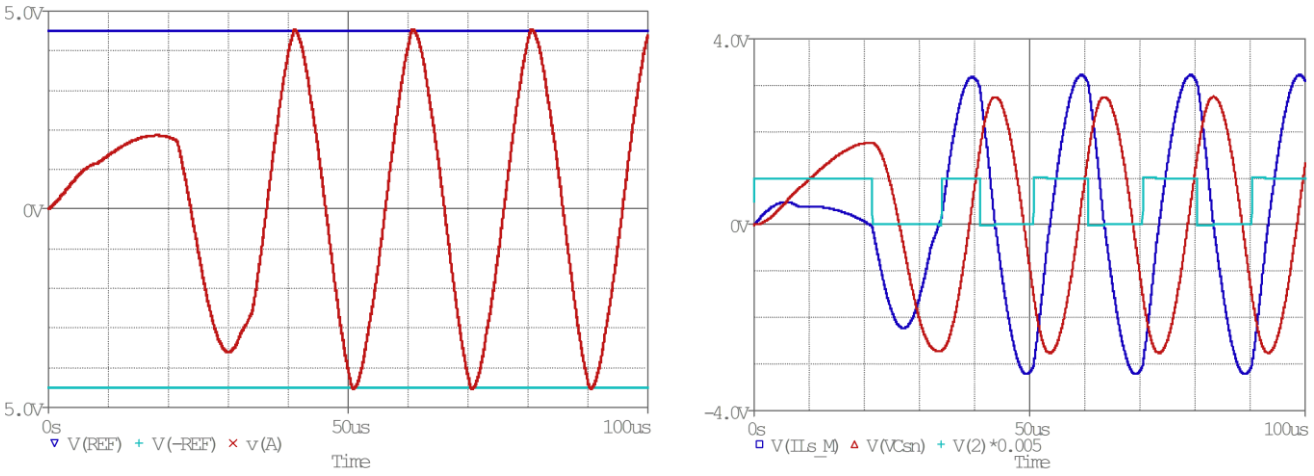
Table 3. A comparison between theoretical and simulation results of control characteristics $I'_0(Ref)$.

Control Parameter *Ref*	I'_{0simul}	I'_{0calc}	Relative Error δ, %
0.5	0.196	0.181	8.160
1.0	0.409	0.394	3.973
1.5	0.634	0.618	2.579
2.0	0.863	0.846	1.945
2.5	1.091	1.074	1.557
3.0	1.320	1.304	1.253
3.5	1.548	1.532	1.048
4.0	1.777	1.761	0.859
4.5	2.004	1.990	0.737
5.0	2.232	2.218	0.631
5.5	2.459	2.447	0.517
6.0	2.687	2.674	0.465
6.5	2.914	2.904	0.345
7.0	3.140	3.131	0.314
7.5	3.367	3.360	0.221

The differences demonstrated in Figure 12 can be explained by the assumptions made for the needs of the theoretical analysis.

5.2. Dynamic Response Simulation Results

The simulation waveforms shown in Figure 13 illustrate the converter's behavior at start-up for induction ratio $a = 3$.



(**a**) (**b**)

Figure 13. Simulation waveforms of the control circuit signals at start-up ($a = 3$; $Ref = 4.5$; $V_0 = 100$V): (**a**) Simulation waveforms of the signals v (REF), v(A) and v(−REF); (**b**) Simulation waveforms of the normalized values of signals v(VCsn), v(ILs_M) and v(2).

In this case, due to the significant value of the control parameter *Ref*, the state trajectory did not reach a control line for some time interval. Moreover, the controlled switches conducted an entire half-period as the inverter voltage and current across the inductance *Ls* (VILs_M) were in phase. The converter operated at a frequency equal to the resonant ω_0.

Figure 14 shows the simulation results in the phase plane when the converter is started at a control parameter $Ref = 4.5$.

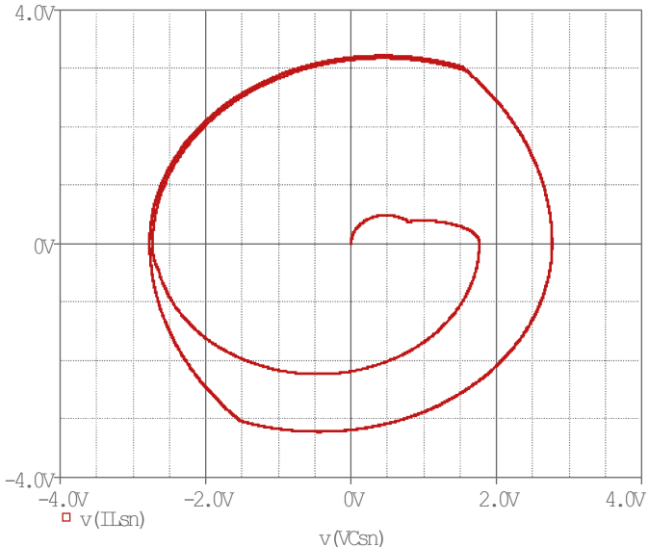


Figure 14. Converter's response at start-up (a = 3; Ref = 4.5; V_0 = 100 V).

The dynamic response of the converter in the case of a significant increase or decrease in the control parameter Ref is demonstrated by the state trajectories in Figures 15 and 16, respectively. Figure 15 illustrates that as the control parameter Ref increased (from Ref = 3 to Ref = 4.5), the energy in the resonant circuit was built up by the series conduction of the transistors. It is known from the [22] that the rate at which the tank energy can change within half a cycle is limited. The new steady state takes place for more than a half-cycle.

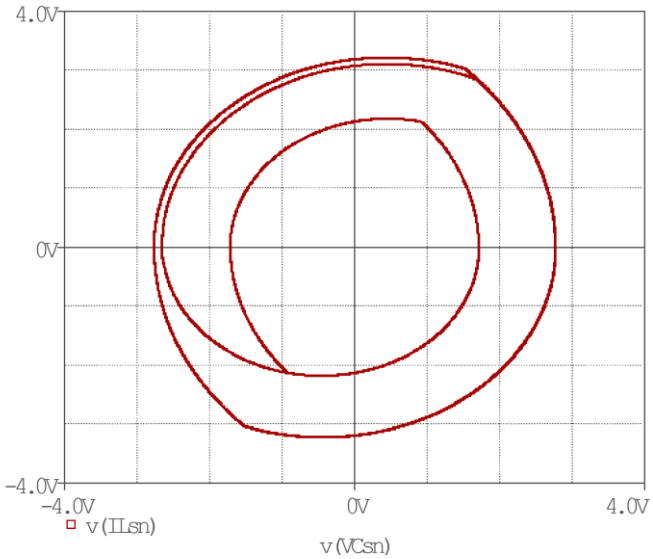


Figure 15. Converter's response at increasing the control parameter (from Ref = 3 to Ref = 4.5), a = 3 and V_0 = 100 V.

Similarly, Figure 16 shows the circuit's response when the control parameter Ref decreased (from Ref = 4.5 to Ref = 3). Thus, the resonant circuit's energy was reduced by conductions of freewheeling diodes.

The results presented in the two figures (Figures 15 and 16) show that in both cases, the system reached the new target trajectory in the minimum time, determined only by the inherent properties of the converter. Thus, the proposed simplified control technique fully utilized the potential of the simple optimal trajectory control method for fast converter response according to the load requirements.

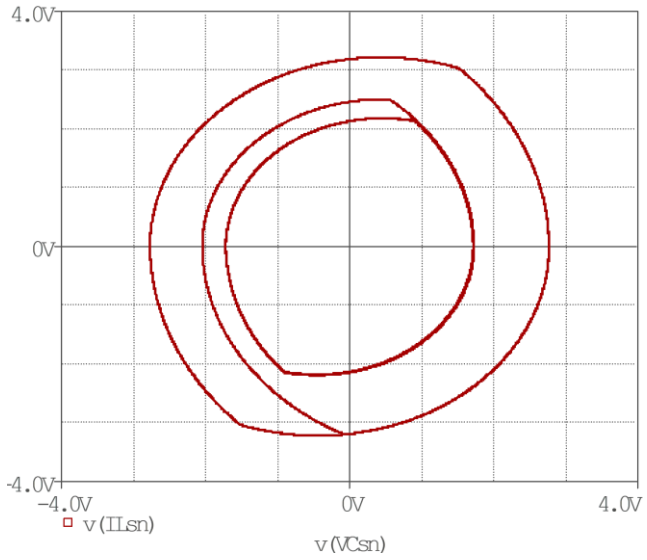


Figure 16. Converter's response at decreasing the control parameter (from *Ref* = 4.5 to *Ref* = 3), $a = 3$ and $V_0 = 100$ V.

The performed studies through the model confirm that the considered control technique provides a fast dynamic response and stable converter operation even when the control parameter changes abruptly.

The dynamic performance of the investigated simple control method under short-circuit is shown in Figure 17.

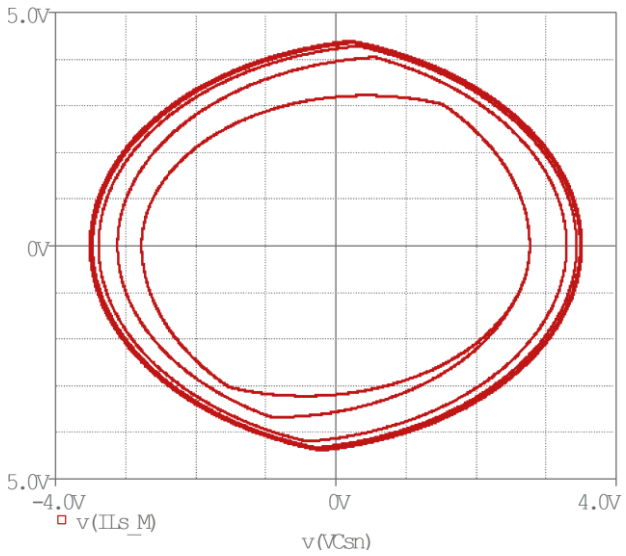


Figure 17. Converter's response at load short-circuit (*Ref* = 4.5; $a = 3$, $V_0 = 100$ V—before short-circuit occurs).

Within a short time, the system abruptly reached another target trajectory. The phase representation shows that the new energy level was not much greater than the previous steady-state level. Thus, the assertion that the converter had a behavior of current source stable at short-circuit mode was proven.

6. Conclusions

The application of a simple control method for a resonant LLC DC-DC converter based on a linear combination of the voltage across the capacitor and the current through the

inductance in the series resonant circuit was discussed. Furthermore, the power transistors switched at zero voltage. The performed theoretical analysis showed that the converter's control provided linear regulation characteristics and behaved like a stable current source at a short-circuit and the output current's value did not depend on the inductance ratio, thus confirming that the behaviors of the LLC resonant converter were similar to those of the optimal trajectory control but using simpler implementation.

The boundaries, at which the simple trajectory control method was valid, were defined. The stability border on the output characteristics outlined a theoretical possibility whereby the normalized output voltage achieved a relatively high value (≈0.8) as the control parameter *Ref* varied considerably. Moreover, this voltage increased insignificantly when the inductance ratio decreased. The area of the discontinuous current mode increased when decreasing the value of inductance ratio a.

The control characteristics $I'_0(Ref)$ were near linear for values of the control parameter $Ref \geq 1$. On the basis of the tabular results for the values of the dynamic gain $\Delta I'_0/\Delta Ref$, it can be concluded that at low values of the normalized output voltage (V'_0= 0.1÷0.3) the control characteristics practically coincide, regardless of the magnitude of the inductance ratio. For high values of the normalized output voltage (V'_0 = 0.6÷0.7), the differences between the control characteristics at inductance ratios a = 3 and $a = \infty$ were insignificant (0.01–0.02), whereas those obtained at inductance ratio a = 1 deviated significantly (0.04–0.08).

Regarding the dependences of the average value of the input current $I'_d(I'_0)$, it was observed (the reading taken of the stability border) that when parameter *Ref* was changed from 3.5 to 5.0 the output power in relative units increased by approximately 1.49 times for a = 1. Respectively, for a = 3, this increase was 1.41 times and for $a = \infty$ it was 1.39 times. Therefore, even for low values of the inductance ratio, the considered circuit had very similar properties to those of a series resonant converter.

The properties and dynamic behavior of the converter were verified using computer simulations, both in steady state and when the control parameter was changed significantly. The proposed functional model of the control system was composed of a minimum number of elements and was easy to set up.

A comparison between theoretical and simulation results of output characteristics $V'_0(I'_0)$ showed relative error within 2%. More significant differences (around 3%) were observed for small values of the control parameter *Ref*. Regarding the comparison between theoretical and simulation results of control characteristics $I'_0(Ref)$, it could be pointed out that the deviations between theoretical and simulation results did not exceed 2%. For small values of the control parameter *Ref*, greater disparities were observed. A growing tendency of the relative error was observed as zero was approached.

Additionally, calculating the value of the voltage applied to the capacitor of the series resonant circuit would be very convenient when applying the considered control method to some half-bridge circuits. Moreover, using only one measurement is a prerequisite for increasing the reliability of the proposed solution. The performed studies using the model confirm that the simplified control technique provides a fast dynamic response and robust operation when the control parameter is changed. Therefore, the converter can be successfully used as a battery-charging device.

Author Contributions: T.G. and A.V. were involved in the full process of producing this paper, including conceptualization, methodology, modeling, validation, visualization and preparing the manuscript. All authors have read and agreed to the published version of the manuscript.

Funding: This research received no external funding.

Data Availability Statement: Not applicable.

Acknowledgments: The authors would like to thank the Research and Development Sector at the Technical University of Sofia for the financial support.

Conflicts of Interest: The authors declare no conflict of interest.

References

1. Bughneda, A.; Salem, M.; Alhuyi Nazari, M.; Ishak, D.; Kamarol, M.; Alatai, S. Resonant Power Converters for Renewable Energy Applications: A Comprehensive Review. *Front. Energy Res.* **2022**, *10*, 846067. [CrossRef]
2. Madzharov, N.; Iliev, D. Design and Regulation of the HF Inverter for Contactless Power Transfer Systems. In Proceedings of the 2020 55th International Scientific Conference on Information, Communication and Energy Systems and Technologies (ICEST), Niš, Serbia, 10–12 September 2020; pp. 133–136. [CrossRef]
3. Vuchev, S.; Arnaudov, D. Characteristics and design of a resonant DC-DC converter based modular topology for electric vehicle fast charging. In Proceedings of the 2019 International Exhibition and Conference for Power Electronics, Intelligent Motion, Renewable Energy and Energy Management, PCIM Europe, Nuremberg, Germany, 7–9 May 2019; pp. 1782–1789.
4. Deshmukh, S.; Iqbal, A.; Islam, S.; Khan, I.; Marzband, M.; Rahman, S.; Al-Wahedi, A.M. Review on classification of resonant converters for electric vehicle application. *Energy Rep.* **2022**, *8*, 1091–1113. [CrossRef]
5. Vu, H.-N.; Choi, W. A Novel Dual Full-Bridge LLC Resonant Converter for CC and CV Charges of Batteries for Electric Vehicles. *IEEE Trans. Ind. Electron.* **2018**, *65*, 2212–2225. [CrossRef]
6. Jagadan, G.; Sourav, U.K.; Chathayil, V.; Kumar, R.S.; Manjunath, V. Design of LLC Resonant Converter for High Efficiency EV Charging. In Proceedings of the 2022 IEEE Global Conference on Computing, Power and Communication Technologies (GlobConPT), New Delhi, India, 23–25 September 2022; pp. 1–7. [CrossRef]
7. Kim, D.-H.; Kim, M.-S.; Hussain Nengroo, S.; Kim, C.-H.; Kim, H.-J. LLC Resonant Converter for LEV (Light Electric Vehicle) Fast Chargers. *Electronics* **2019**, *8*, 362. [CrossRef]
8. Han, J.-H.; Lim, Y.-C. Design of an LLC Resonant Converter for Driving Multiple LED Lights Using Current Balancing of Capacitor and Transformer. *Energies* **2015**, *8*, 2125–2144. [CrossRef]
9. Wang, Y.; Guan, Y.; Ren, K. A single-stage LED driver based on BCM boost circuit and LLC converter for street lighting system. *IEEE Trans. Ind. Electron.* **2015**, *62*, 5446–5457. [CrossRef]
10. Zeng, J.; Zhang, G.; Yu, S.S.; Zhang, B.; Zhang, Y. LLC resonant converter topologies and industrial applications—A review. *Chin. J. Electr. Eng.* **2020**, *6*, 73–84. [CrossRef]
11. An Introduction to LLC Resonant Half-Bridge Converter. Available online: https://www.st.com/resource/en/application_note/an2644-an-introduction-to-llc-resonant-halfbridge-converter-stmicroelectronics.pdf (accessed on 15 September 2008).
12. Park, H.-P.; Kim, M.; Jung, J.-H. A Comprehensive Overview in Control Algorithms for High Switching-Frequency LLC Resonant Converter. *Energies* **2020**, *13*, 4455. [CrossRef]
13. Wei, Y.; Woldegiorgis, D.; Mantooth, A. Control Strategies Overview for LLC Resonant Converter with Fixed Frequency Operation. In Proceedings of the 2020 IEEE 11th International Symposium on Power Electronics for Distributed Generation Systems (PEDG), Dubrovnik, Croatia, 28 September–1 October 2020; pp. 63–68. [CrossRef]
14. Tayebi, S.M.; Hu, H.; Abdel-Rahman, S.; Batarseh, I. Dual-input single-resonant tank LLC converter with phase shift control for PV applications. *IEEE Trans. Ind. Appl.* **2019**, *55*, 1729–1739. [CrossRef]
15. Guo, B.; Zhang, Y.; Zhang, J.; Gao, J. Hybrid Control Strategy of Phase-Shifted Full-Bridge LLC Converter Based on Digital Direct Phase-Shift Control. *J. Power Electron.* **2018**, *18*, 802–816. [CrossRef]
16. Kim, J.; Kim, C.; Kim, J.; Lee, J.; Moon, G. Analysis on load-adaptive phase-shift control for high efficiency full-bridge LLC Resonant converter under light-load conditions. *IEEE Trans. Power Electron.* **2016**, *31*, 4942–4955. [CrossRef]
17. Grigorova, T.; Vuchev, A. A Study of a Phase-Shifted Full-Bridge LLC Resonant Converter Operating in Continuous Conduction Mode with ZVS. In Proceedings of the 2022 13th National Conference with International Participation (ELECTRONICA), Sofia, Bulgaria, 19–20 May 2022; pp. 1–6. [CrossRef]
18. Chen, W.; Liu, K.; Zhao, J.; Jin, C. Dynamic improvement for phase-shift LLC resonant converter based on disturbance observer. *Energy Rep.* **2023**, *9* (Suppl. 1), 1018–1025. [CrossRef]
19. Zhou, K.; Liu, Y.; Wu, X. Research on Wide Input Voltage LLC Resonant Converter and Compound Control Strategy. *Electronics* **2022**, *11*, 3379. [CrossRef]
20. Pan, H.; He, C.; Ajmal, F.; Chen, H.; Chen, G. Pulse-width modulation control strategy for high efficiency LLC resonant converter with light load applications. *IET Power Electron.* **2014**, *7*, 2887–2894. [CrossRef]
21. Hu, Z.; Liu, Y.-F.; Sen, P.C. Bang-Bang Charge Control for LLC Resonant Converters. *IEEE Trans. Power Electron.* **2015**, *30*, 1093–1108. [CrossRef]
22. Oruganti, R.; Yang, J.J.; Lee, F.C. Implementation of optimal trajectory control of series resonant converter. *IEEE Trans. Power Electron.* **1988**, *3*, 318–327. [CrossRef]
23. Feng, W.; Lee, F.C.; Mattavelli, P. Optimal Trajectory Control of LLC Resonant Converters for LED PWM Dimming. *IEEE Trans. Power Electron.* **2014**, *29*, 979–987. [CrossRef]
24. Feng, W.; Lee, F.C.; Mattavelli, P. Simplified Optimal Trajectory Control (SOTC) for LLC Resonant Converters. *IEEE Trans. Power Electron.* **2013**, *28*, 2415–2426. [CrossRef]
25. Nabih, A.; Ahmed, M.; Li, Q.; Lee, F.C. Simplified Optimal Trajectory Control for 1 MHz LLC Converter with Wide Input Voltage Range. In Proceedings of the 2019 IEEE Applied Power Electronics Conference and Exposition (APEC), Anaheim, CA, USA, 17–21 March 2019; pp. 212–219. [CrossRef]
26. Rossetto, L. A Simple Control Technique for series resonant converter. *IEEE Trans. Power Electron.* **1996**, *11*, 554–560. [CrossRef]

27. Vuchev, A.S.; Grigorova, T. State Plane Analysis of an LLC DC-DC Converter Operating above the Resonant Frequency. In Proceedings of the 2021 12th National Conference with International Participation (ELECTRONICA), Sofia, Bulgaria, 27–28 May 2021; pp. 1–4. [CrossRef]
28. Vuchev, A.; Grigorova, T.; Vuchev, S. Analysis of Continuous Current Mode of an LLC Resonant DC-DC Converter at ZVS. In Proceedings of the 2022 13th National Conference with International Participation (ELECTRONICA), Sofia, Bulgaria, 19–20 May 2022; pp. 1–4. [CrossRef]
29. PSPICE-FOR-TI PSpice®for TI Design and Simulation. Available online: https://www.ti.com/tool/PSPICE-FOR-TI#downloads (accessed on 15 September 2020).
30. Williams, I. Pspice for TI Texas Instruments, Getting Started with the New PSpice®for TI Design and Simulation Tool. Available online: https://www.ti.com/lit/ml/slyp725/slyp725.pdf?ts=1686213827934&ref_url=https%253A%252F%252Fwww.google.com%252F (accessed on 16 December 2020).
31. Ahn, S.-H.; Gong, J.-W.; Jang, S.-R.; Ryoo, H.-J.; Kim, D.-H. Design and implementation of enhanced resonant converter for EV fast charger. *J. Electr. Eng. Technol.* **2014**, *9*, 143–153. [CrossRef]

Disclaimer/Publisher's Note: The statements, opinions and data contained in all publications are solely those of the individual author(s) and contributor(s) and not of MDPI and/or the editor(s). MDPI and/or the editor(s) disclaim responsibility for any injury to people or property resulting from any ideas, methods, instructions or products referred to in the content.